Geofluids
August 2016, Volume 16, Issue 3, Pages 476-489
http://dx.doi.org/10.1111/gfl.12169
http://archimer.ifremer.fr/doc/00314/42514/

Modeling of hydrogen production by serpentinization in ultramafic-hosted hydrothermal systems: Application to the Rainbow field

Mügler C. [1, *], Jean-Baptiste P. [1], Perez Florian [1, 2], Charlou Jean-Luc [2]

[1] Laboratoire des Sciences du Climat et de l'Environnement; UMR 8212 CEA-CNRS-UVSQ, Orme des Merisiers; 91191 Gif-sur-Yvette Cedex France
[2] IFREMER Brest; Département Géosciences Marines; 29280 Plouzané France

* Corresponding author : C. Mügler, Tel: +33 1 69089363; Fax: +33 1 69087716 ;
email address : claude.mugler@cea.fr

Abstract :

The production of hydrogen by serpentinization in ultramafic-hosted hydrothermal systems is simulated by coupling thermodynamic and dynamic modeling in the framework of a thermo-hydraulic single-pass model where a high-temperature hydrothermal fluid moves preferentially through a main canal of high permeability. The alteration of ultramafic rocks is modeled with a first-order kinetic formulation, wherein the serpentinization rate coefficient, Kr, takes the form: Kr = A exp(−α(T − T0)2). In this formulation, α determines the temperature range of the reaction and T0 is the temperature at which the serpentinization rate reaches its maximum. This model is applied to the Rainbow hydrothermal system, which is situated on the Mid-Atlantic Ridge, and characterized by a high temperature, a high mass flux, and a very high hydrogen concentration. The results show that a first-order kinetic law gives a useful representation of the kinetics of serpentinization. The estimated value for the parameter A in the temperature-dependent formulation of the serpentinization rate coefficient lies in the range (1–5) × 10−11 s−1. This effective parameter is several orders of magnitude lower than the values obtained from small grain-size experiments, but in agreement with other published modeling studies of natural systems. Numerical simulations show that the venting site is able to produce the observed high concentration of hydrogen during the whole continuous lifetime of the Rainbow site.

Keywords : first-order kinetic law, hydrothermal system, Rainbow vent site, reaction rate, serpentinization

INTRODUCTION

Hydrothermal activity along the axes of Mid-Ocean Ridges (MOR) is a key driver of energy and matter transfer from the interior of the Earth to the ocean floor. Seawater penetrates the permeable young crust, warms at depth, and reacts with the surrounding mantle rocks. At slow spreading MOR, this interaction can produce large volumes of serpentinized peridotite. Serpentinization of peridotite is an exothermic hydration process in which an assemblage of olivines $(MgFe)_2SiO_4$ and pyroxenes (both orthopyroxenes $(MgFe)(SiO_3)$ and clinopyroxenes $Ca(MgFe)(SiO_3)_2$) undergoes hydration to hydrous silicates (e.g., serpentine $(MgFe)_3Si_2O_5(OH)_4$), iron oxides (magnetite Fe_3O_4), and other alteration products such as brucite $(MgFe)(OH)_2$ and talc $(MgFe)_3Si_4O_{10}(OH)_2$ (Moody 1976, Frost 1985, MacDonald & Fyfe 1985, Janecky & Seyfried Jr. 1986). The extreme reducing conditions that prevail during the hydrothermal alteration of ultramafic rocks promote the formation of hydrogen through the reaction of water with ferrous iron-rich minerals contained in the rocks, primarily olivine and pyroxene: Ferrous iron (Fe^{2+}) is oxidized by the water to ferric iron (Fe^{3+}), which typically precipitates as magnetite; while H_2O is reduced to H_2. H_2 generation during serpentinization of olivine (the main mineral in most ultramafic rocks) can be represented by the general reaction (Klein et al. 2013):

$$\underset{\text{olivine}}{(MgFe)_2SiO_4} + \underset{\text{water}}{\alpha_1 H_2O} \rightarrow \underset{\text{brucite}}{\alpha_2(MgFe)(OH)_2} + \underset{\text{serpentine}}{\alpha_3(MgFe)_{3\text{-}Fe(III)}(SiFe)_{2\text{-}Fe(III)}O_5(OH)_4} + \underset{\text{magnetite}}{\alpha_4 Fe_3O_4} + \underset{\text{hydrogen}}{\alpha_5 H_2} \qquad (1)$$

The serpentine mineral group encompasses a variety of polymorphs such as lizardite, antigorite, chrysotile. The nature and the amount of the reaction products depend on the proportion of olivine and pyroxene in the initial peridotite, on the pressure and temperature conditions, on the ratio between the initial mass of water and the initial mass of rock (water/rock ratio, denoted *w/r*), and also on the fluid composition and on the evolution of the system composition. McCollom & Bach (2009) used numerical models based on chemical thermodynamics to examine the impact of the temperature and the *w/r* ratio on the H_2 generation during serpentinization. Thermodynamic modeling was performed at equilibrium conditions and the influence of kinetics was neglected. However, it is widely recognized that the kinetics of the dissolution of olivine controls the speed of serpentinization, and thus the production of hydrogen (Marcaillou et al. 2011, Malvoisin et al. 2012).

Martin & Fyfe (1970) investigated the reaction kinetics of serpentinization. They performed experiments with synthetic powders of olivine (forsterite Mg_2SiO_4) and pyroxene (enstatite $MgSiO_3$), at temperatures between 100°C and 560°C, and at a pressure of 140 MPa. The initial grain diameters were between 58 and 79 µm. The *w/r* ratio varied between 0.17 and 0.40. The maximum reaction rate occurred at $T \sim 270°C$, and tended to zero at $T<150°C$ or $T>375°C$, where the mineral alteration effectively stopped. The reaction rates obtained with a mixture of olivine and pyroxene were very similar. These results were confirmed by the experiments performed by Wegner & Ernst (1983) with a synthetic forsterite.

The *w/r* ratios used in these laboratory experiments were slightly lower than the *w/r* value considered in the context of natural serpentinization by Agrinier & Cannat (1997). However, until 2011, the experimental results of Martin & Fyfe (1970) were the only ones available for modeling the reaction rate of serpentinization. As a consequence, they have been widely used (Allen & Seyfried Jr. 2004, Emmanuel & Berkowitz 2006, Delescluse & Chamot-Rooke 2008, Iyer et al. 2010, Rudge et al. 2010). Several authors parameterized the experimental data of Martin & Fyfe (1970) by a bell-shaped curve for the reaction rate coefficient, K_r, of the form:

$$\mathrm{K_r} = \mathrm{A}\exp\left(-\alpha\left(\mathrm{T}-\mathrm{T_0}\right)^2\right). \tag{2}$$

In this equation, α determines the temperature range of the reaction, and T_0 is the temperature at which the serpentinization rate reaches its maximum. Emmanuel & Berkowitz (2006) estimated $\alpha = 2.5\times10^{-4}$°C^{-2}, $T_0 = 270$°C, and $A = 2\times10^{-6}$ s^{-1}, although Kelemen & Matter (2008) used $\alpha = 2.09\times10^{-4}$°C^{-2}, $T_0 = 260$°C, and $A = 10^{-6}$ s^{-1}. The parameters α and T_0 in Eq. (2) are well constrained by the experimental data, but the rate parameter (i.e. *A*) that ultimately fixes the magnitude of K_r in natural systems remains largely undetermined.

In a more recent experimental study, Marcaillou et al. (2011) investigated the alteration of powdered natural peridotite (1 µm grain-size lherzolite) in pure water at 300°C and 30 MPa, with a *w/r* ratio of 3/2. The reaction rate was successfully modeled by the first-order kinetic formulation Eq. (2) with $A = 5\times10^{-7}$ s^{-1} (Fig.2, Marcaillou et al. 2011).

Based on experiments performed at 50 MPa on powders of natural olivine with a grain size of 1-150 µm, and a *w/r* ratio of 0.4, Malvoisin et al. (2012) proposed a mathematical formulation of the serpentinization kinetics which is more complicated than the first-order kinetics obtained in previous studies (Martin & Fyfe 1970, Marcaillou et al. 2011), and contains four parameters that have to be calibrated.

Ogasawara et al. (2013) also conducted serpentinization experiments at 250°C and 3.98 MPa using olivine and orthopyroxene powders with a grain-size of 25-125 µm. They obtained very high reaction rate coefficients, which may be due to the very high initial porosity in the experiments (~0.5). Furthermore, the reaction rate constant was one order of magnitude higher in the olivine zone ($K_r = 4.4\times10^{-4}$ s^{-1}) than in the orthopyroxene zone ($K_r = 2\times10^{-5}$ s^{-1}). In marked contrast with these results, other laboratory experiments on natural rock samples showed that orthopyroxene reacts significantly faster than olivine at a temperature of ~300°C (Klein et al. 2015). The kinetics of serpentinization were also experimentally determined by Seyfried et al. (2007) and Okamoto et al. (2011).

All these experiments have been performed with powders, raising the question of whether these results are still valid under the *in situ* conditions prevailing at MOR. Malvoisin et al. (2014) showed that the serpentinization kinetics of olivine aggregates is two to three orders of magnitude slower than those measured in the same conditions on powders: A~10^{-9} s^{-1} for olivine aggregates (size~3.5 mm), and A~$(0.1\text{-}1)\times10^{-6}$ s^{-1} for olivine powders (grain size~1-150 µm). We can imagine that the value of A in natural systems should be even lower, due to the much lower reactive surface area of *in situ* coarse-grained ultramafic rock.

Rudge et al. (2010) slightly modified the parameterization of the rate coefficient, K_r, given by Kelemen & Matter (2008), in order to introduce surface area effects:

$$\mathrm{K_r} = \mathrm{K_0}\left(\frac{\mathrm{a_0}}{\mathrm{a}}\right)^2 \exp\left(-\alpha\left(\mathrm{T}-\mathrm{T_0}\right)^2\right), \tag{3}$$

i.e., $A = K_0\times(a_0/a)^2$. In this formulation, a_0 is the grain size ($58\ \mu m \leq a_0 \leq 79\ \mu m$) in the experiments by Martin & Fyfe (1970), and the factor $(a_0/a)^2$ reflects the scaling due to surface area effects, where a is the typical grain size controlling the reaction. As in Eq. (2), T_0 is the temperature at which the serpentinization rate reaches its maximum, and K_0 ~10^{-6} s^{-1} is the corresponding peak rate for a grain size a_0 =70 μm (Kelemen & Matter 2008). Based on the assumption that the typical grain size of peridotite was around a ~ 0.1 mm, Rudge et al. (2010) adopted the value $A \sim 5\times10^{-7}$ s^{-1}. This value of A is in agreement with the rates of olivine serpentinization (A~(0.1-1)×10^{-6} s^{-1}) for powders with grain sizes in the range ~1-150 μm as measured in the experiments performed by Malvoisin et al. (2012). For aggregates with a size of ~3.5 mm, Eq. (3) yields $A \sim 4\times10^{-10}$ s^{-1}. Here again, this value is of the same order of magnitude as the value obtained from experiments, $A \sim 10^{-9}$ s^{-1}, by Malvoisin et al. (2014).

But how can the value of this typical grain size be determined in a natural hydrothermal system? Furthermore, is this parameter meaningful? Although the data from the experiments on powders or aggregates can be used to quantitatively constrain the serpentinization rates in closed systems under constant conditions, the validity of applying these results to natural hydrothermal systems is not so evident. Indeed, these experiments were performed with a static fluid in contact with the rock, in a closed container. In oceanic hydrothermal systems, seawater flows through the rock. This motion can modify chemical reactions, and transport chemical species and heat. The value of the serpentinization rate could also increase or decrease during mineral alteration, depending on crystal grain size and geometry. Furthermore, serpentinization induces volumetric strains, which can result in mechanical fracturing of the ultramafic rock (MacDonald & Fyfe 1985). Such fracturing complicates the dynamics further by continually exposing fresh reactive surfaces. Both the closure of existing fractures and the generation of new fractures are phenomena that have been documented by two types of evidence, viz. by observations in nature and by observations in experiments during serpentinization (Andreani et al. 2004, Iyer et al. 2008a, Iyer et al. 2008b). For example, Andreani et al. (2004) explained the characteristics of serpentine banded veins at different scales by a crack-seal type process of formation, and Iyer et al. (2008b) presented some fracture patterns generated by the serpentinization of ultramafic rocks. On one hand, such volume expanding reaction may clog the pore space, reduce permeability, and limit the transport of fluids. On the other hand, generation of fractures may contribute to an acceleration of the hydration rate, by the production of both fresh reactive surfaces and new pathways for the infiltrating fluids. Jamtveit et al. (2000) presented both field observations and a simple network model to demonstrate how the transport of fluids into initially dry rock can be accelerated by perturbations in the local stress field due to reactions with fluids. More recently, the physical processes involved in this positive feedback were modeled and applied to the carbonation and serpentinization of peridotite (Rudge et al., 2010, Kelemen & Hirth 2012, Plümper et al. 2012).

For all these reasons, it is expected that the value of the parameter A in natural systems is very different from those obtained from small-scale experiments. For example, a value of A=10^{-10} s^{-1} was used by Emmanuel & Berkowitz (2006) to model serpentinization at the Lost City site. Using seismic velocity as a proxy for the integrated progress of all serpentinization reactions, Skelton et al. (2005) obtained time-averaged dissolution rates of $A=(0.2\text{-}2)\times10^{-12}$ s^{-1} for orthopyroxene and olivine, and $A=(0.2\text{-}2)\times10^{-13}$ s^{-1} for clinopyroxene.

In this study, we establish a hydrogeological and geochemical model for describing and quantifying the hydrogen production associated with the serpentinization process in natural ultramafic-hosted hydrothermal systems. Our main objective is to see if the high hydrogen concentrations measured in the hydrothermal fluids of the Rainbow site (MAR) can be reproduced on the basis of simple assumptions regarding the thermo-hydraulic and geochemical functioning of the hydrothermal system, and to derive a field scale value for the serpentinization rate that could be of interest for other hydrothermal environments.

In the following, we first present the Rainbow hydrothermal system, discovered by German et al. (1996) on the Mid-Atlantic Ridge (MAR). The circulation of the Rainbow hydrothermal fluids has been studied recently by Perez et al. (2013) using a thermo-hydraulic model. The large number of data (both from *in situ* measurements and modeling studies) that are available for this site, together with its high hydrogen production rate, render it an excellent study case to test our hydrogen production model. Modeling H_2 production and transport processes can help to reach a better understanding of the functioning of this ultramafic-hosted hydrothermal system.

Then, we present the modeling approach. In this study, we assume that the reaction zone at Rainbow is entirely peridotite. The purpose of our chemical transport model is to determine if *in situ* serpentinization could produce such high quantities of hydrogen from hydrothermal alteration of peridotite. It also allows us to test the validity of applying the first-order kinetic law in modeling serpentinization and the concomitant hydrogen production at the scale of a natural hydrothermal system. The results are presented and discussed in the last section.

RAINBOW VENT SITE DATA

Meaningful mathematical and computational models of seafloor hydrothermal circulation and geochemistry should be able to account for all relevant physical/chemical processes at stake and for all the available data that have been obtained from *in situ* measurements. The latter are putting constraints on the models. The available data vary widely from one vent field to the other, and in general the ability to formulate detailed mathematical and computational models of any particular vent field is limited by a lack of data. The temperature, the hydrogen concentration and the mass flux in the venting zone are of fundamental importance for models of a high-temperature ultramafic hydrothermal site. For this reason, we have applied our modeling approach to the Rainbow site.

The Rainbow hydrothermal vent field was discovered in 1994 (German et al. 1996). It is located south of the Azores at 36°13.8’N-33°54.15’W, at a depth of 2275-2335 m. It is a vigorous ultramafic-hosted hydrothermal system that emits hot fluids over a 20,000 m^2 area from about ten major groups of extremely active black smokers located on an isolated sulfide mound (Thurnherr & Richards 2001, Jean-Baptiste et al. 2004, German et al. 2010). The Rainbow vent fluids have the highest temperature reported for MAR fluids (~360°C), the highest chloride concentration (greater than 750 mM), the lowest end-member pH (2.8), and the highest trace metal contents (Fe, Cu, Zn); they also have high K, Rb and Cs contents (Charlou et al. 2010). One of the most interesting characteristics of the fluids emitted by the active chimneys of the Rainbow vent site is their very high hydrogen concentration (up to 16 mmol kg^{-1}) (Charlou et al. 2002, 2010, Seyfried et al. 2011). The unique physical and chemical characteristics of the Rainbow site have raised numerous questions about the processes at work. The low-pH and high-temperature fluids issuing from the vents at Rainbow indicate that the rates of olivine hydrolysis must be slow and that an intermittent magmatic heat source must be present in its near proximity, because it is otherwise impossible to account for the high temperature and the high flow rates observed at this site (Allen & Seyfried Jr. 2004). The cause of the high hydrogen concentrations is still under debate (McCaig et al. 2007, Charlou et al. 2010, Seyfried et al. 2011).

The active venting area contains numerous active and inactive sulfide chimneys that lie on top of sulfide mounds built up mostly by the accumulation of collapsed, dead chimneys (Marques et al. 2006). A radiochemical study of the massive sulfides from the Rainbow hydrothermal site suggested that there was a first period of activation about 23,000 ± 1,500 years ago, followed by two periods of reactivation 3,200 and 2,000 years ago. This result gives an estimation of the age of the high-temperature hydrothermal activity, and shows the stability of the emplacement of the vent field (Kuznetsov et al. 2006). ^{14}C dating of the shells confirmed that the hydrothermal activity in the Rainbow area began at least ~25,500 years BP (Lartaud et al. 2010). Radiocarbon dating of a core collected close to the vent site indicates that both the concentration and the flux of hydrothermally derived material increased significantly at some time between 8,000 and 12,000 years ago (Cave et al. 2002). This variation may reflect the initiation or intensification of hydrothermal venting at the Rainbow hydrothermal field at this time, perhaps linked to some specific tectonic event. Hydrothermal precipitates from the TAG hydrothermal field, which is located further north on the MAR, also indicate a long history of high-temperature activity; and that at the currently active TAG mound, episodic high-temperature venting has occurred every few thousand years, with current activity beginning ~80 years ago (Lalou et al. 1998, Lowell & Germanovitch 2004). Models of hydrothermal heat extraction from a convecting crystallizing magma chamber showed that relatively rapid amounts of magma replenishment would be needed to maintain observed hydrothermal heat output on a decadal time scale (Liu & Lowell 2009, Lowell et al. 2013). Hence, although the age of the high-temperature hydrothermal Rainbow field is several thousands of years, its functioning is certainly intermittent, and its continuous lifetime may be only tens to hundreds of years.

Since the first analyses of vent fluid samples (Charlou et al. 1998), the chemistry and temperature of the active vents have remained stable for more than a decade (Douville et al. 2002, Charlou et al. 2002, Charlou et al. 2010, Seyfried et al. 2011). Furthermore, the homogeneity of both the chemistry and temperature of the vent fluids has brought the authors to the assumption that all smokers at this vent site have a single common fluid source, and that there is a magmatic body residing deep underneath (Charlou et al. 2010, Seyfried et al. 2011).

The vent fluids of the ultramafic-hosted Rainbow hydrothermal system do not only exhibit high temperature, unique chemistry and long duration of venting, but they also have high rates of fluid flow. Based on the ^{3}He budget of the site, the estimated mass flux of high-temperature fluid exiting at the Rainbow vent field is W_u = 490 ± 220 kg s^{-1} (Jean-Baptiste et al. 2004, German et al. 2010). This corresponds to a heat flux of 1320±600 MW (Jean-Baptiste et al. 2004), and is in agreement with the earlier estimates of Thurnherr & Richards (2001), based on hydrographic considerations: 2300±2000 MW. This high heat output is in the same range as those of the Lucky Strike site: 3800±1200 MW (Jean-Baptiste et al. 1998) and of the TAG site: 1810±693 MW (Wichers et al. 2005), both on the MAR. It is also in excellent agreement with modeled heat fluxes for slow spreading ridges obtained by calculating the available heat from hydrothermal cooling in the neovolcanic zone (Baker 2007). Hence, the estimated mass flux per square meter, Q_u, is constrained as:

$$1.35 \times 10^{-2}\ \mathrm{kg\ s^{-1}\ m^{-2}} < Q_u < 3.55 \times 10^{-2}\ \mathrm{kg\ s^{-1}\ m^{-2}} \qquad (4)$$

The water flux, Q_u, corresponds to a mean mass flux of hot water in the 20,000 m^2-section of the discharge zone of the Rainbow site.

METHOD

Composition of the rock

Rocks with a harzburgitic composition are most representative of ultramafic rocks that are exposed to fluid circulation beneath the seafloor at slow spreading ridges (Allen & Seyfried Jr. 2003). Accordingly, we performed calculations with a reactant rock composed of 80 wt% olivine (5.419 moles $Mg_{1.8}Fe_{0.2}SiO_4$ per kg of rock), 15 wt% orthopyroxene (1.427 moles $Mg_{0.85}Fe_{0.15}SiO_3$ kg^{-1}), and 5 wt% clinopyroxene (0.228 moles $CaMg_{0.9}Fe_{0.1}(SiO_3)_2$ kg^{-1}). This composition is the same as the one used by McCollom & Bach (2009). The initial density of the rock (before serpentinization processes start) is ~ 3000 kg m^{-3}. The initial fluid reactant was assumed to be composed of seawater depleted in O_2 and sulphate and partially depleted in Mg and Ca so as to achieve the charge balance (Table 1). This fluid is nominally intended to represent seawater whose composition has been modified by circulation through the crust (McCollom & Bach 2009).

All calculations were performed for a pressure of 35 MPa, which is appropriate for hydrothermal systems such as the Rainbow site.

Thermodynamic modeling

Calculations of the chemical equilibrium were performed using the computer program, EQ3/6, version 8.0 (Wolery 1992), with a customized thermodynamic database compiled using SUPCRT92 (Johnson et al. 1992). Activity coefficients for aqueous species were calculated using the B-dot equation (Helgeson et al. 1981). Chrysotile $Mg_3Si_2O_5(OH)_4$ was used in the calculations to represent the serpentine group. Solid solutions were included in the database for many minerals but only Fe-for-Mg exchange was considered for these solid solutions (McCollom & Bach 2009). Table 2 lists the solid solutions included in the thermodynamic database. Ideal site mixing was assumed for all solid solutions. All these assumptions are the same as those described and justified by McCollom & Bach (2009)

Serpentinization rate

The purpose of our modeling approach is to test the validity of applying the first-order kinetic law for modeling the serpentinization process and the concomitant hydrogen production at the scale of natural systems. We adopt the first-order kinetic formulation of Emmanuel & Berkowitz (2006) for the reaction rate, R, of the alteration of the harzburgite. With this formulation, the rate of serpentinization, $R = -\partial m_r/\partial t$ (where m_r is the mass of harzburgite within a given volume of rock), is a linear function of the reactive surface area, S_r, which is a characteristic of the mass m_r of harzburgite. Hence, $\partial m_r/\partial t = -k S_r$. The units corresponding to the quantities m_r, S_r, and k are kg, m^2, and kg m^{-2} s^{-1}, respectively. During chemical reactions the ratio S_r/m_r may vary but if it is assumed to be constant throughout the serpentinization process it follows:

$$R = -\frac{\partial m_r}{\partial t} = K_r m_r. \qquad (5)$$

We will call hereafter R the serpentinization rate. The rate coefficient K_r can be described by Eq. (2): $K_r = A \exp(-\alpha (T-T_0)^2)$ with $\alpha = 2.5\times10^{-4}{}^\circ C^{-2}$, and $T_0 = 270^\circ C$. We chose this equation for the rate coefficient, instead of the formulation of Malvoisin et al. (2012), because of its simplicity (a small number of parameters) and its robustness. Indeed, this formulation successfully modeled both the experiments of Martin & Fyfe (1970), with $A = 2\times10^{-6}\ s^{-1}$, and the experiments of Marcaillou et al. (2011), with $A = 5\times10^{-7}\ s^{-1}$. We chose to only calibrate the A parameter. In fact, as explained in the introduction, the two parameters α and T_0 (which define the temperature dependence of the reaction rate) are rather well constrained by the experimental data and not expected to be affected by the change of scale from laboratory to *in situ* experiments. Sensitivity tests allowing for uncertainties of a factor of 2 on α and ± 30°C on T_0 show that such uncertainties affect the hydrogen production rate R by ~40% only. This is almost negligible compared to the variations of the parameter A which can be as large as several orders of magnitude depending on grain size.

The *w/r* mass ratio is usually defined as the ratio between the initial mass of water and the initial mass of rock in a closed box. This “static” *w/r* is used to model experiments in thermodynamic equilibrium in closed systems. We previously used this definition to calculate the hydrogen production as a function of the temperature and *w/r*, using a thermodynamic database. In an open system, the static fluid/rock ratio, *w/r*, can be replaced by a “dynamic” ratio, which is expressed as a function of the total mass of fluid, Δm_w, that is involved in the serpentinization of a mass of peridotite, Δm_r, during a given interval of time, Δt (Allen & Seyfried Jr. 2004):

$$\frac{w}{r} = \frac{\Delta m_w/\Delta t}{\Delta m_r/\Delta t} = \frac{W}{R} \qquad (6)$$

where W is the fluid mass flow rate in kg s^{-1}, and R is the serpentinization rate in kg s^{-1}. We will use this “dynamic” water/rock ratio W/R in the following sections for the modeling of production and transport of hydrogen.

The thermo-hydraulic model

In our recent thermo-hydraulic modeling study of the Rainbow site (Perez et al., 2013), we came to the conclusion that a homogeneous permeability field does not exist that would be able to reproduce simultaneously the high exiting temperatures and the high mass flux which characterize the Rainbow site. Instead, we showed that introducing the assumption that the hydrothermal circulation preferentially takes place through a deep high-permeability zone can account for both the high discharge rate and the high temperatures that are observed *in situ* at the vent site. Such a single-pass type of modeling approach has already been adopted in several studies to describe some of the Mid-Ocean-Ridge hydrothermal systems (e.g. Lowell & Germanovich 2004, Lowell et al. 2013). Figure 1 displays a cross-section of the subsurface hydrothermal system modeled. This single-pass configuration is very similar to the two-dimensional geometry described in Fig. 19 of Perez et al. (2013). The main difference is that we used an axially symmetric geometry instead of a two-dimensional one, because this appears to be better adapted to the morphological specificity of the Rainbow site. Indeed, Perez (2012) showed that simulations with an axially symmetric geometry yielded mass fluxes, venting-surface areas, and exiting fluid temperatures that are in better agreement with the values measured than previous 2D simulations. Following Jupp & Schultz 2004, the main characteristics of the geometry and the permeability of the single-pass model can be estimated from the simplified energy and mass balance equations of the system; they are summarized in Table 3 and their uncertainty is discussed in the last section.

The energy and mass balance equations for the fluid flowing through the porous medium are numerically solved with the same computer code (Cast3M code, http://www-cast3m.cea.fr) as the one used and described in Perez et al. (2013). The procedure can be briefly summarized as follows. A first-order implicit-time scheme and a finite-volume method for spatial discretization are used with the BiCGSTAB solver, together with a biconjugate gradient stabilized algorithm for solving non-symmetric systems (Perez et al., 2013). The diffusive part is solved with a finite-volume method using the multipoint flux approximation. For the convective part, the spatial scheme depends on the value of the Peclet number *Pe*: the scheme degenerates into a second-order accuracy centered scheme for dominant diffusion transport ($Pe<2$) and into a first-order upwind scheme for dominant advective transport. The numerical scheme adopted is able to solve highly nonlinear coupled equations both on long and short spatiotemporal scales. The full details have been described in (Perez et al. 2013).

In the thermo-hydraulic simulation, the fluid is initially at rest and the temperature is equal to T_0 in the whole porous domain. The fluid enters at a temperature of T_0 and exits with a zero diffusive heat flux.

The bottom boundary is impermeable, and we use a Dirichlet-type condition for the temperature to model the driver of the convection of the hydrothermal fluids (see Fig. 1). This isothermal lower boundary requires that an infinite reservoir of heat is available to drive the hydrothermal system. Such an assumption is acceptable for short time scales of decades or a few hundreds of years at a low spreading ridge axis (Liu & Lowell 2009; Lowell et al. 2013). We have adopted a mesh inspired by the one used in the previous study of Perez et al. (2013). It is made of 30,751 grid elements. The spatial resolution is coarse in the recharge zone (top right corner of Fig.1) where $\Delta x=20$ m and $\Delta z=30$ m, and increases towards the bottom of the domain and the central discharge zone where $\Delta x=2$ m and $\Delta z=0.5$ m. We have verified that the numerical results are not mesh-dependent.

Transport of hydrogen

After a few decades, the modeled hydrothermal circulation reaches a quasi-steady state. Then, the corresponding temperature and pressure fields are used to simulate the transport of hydrogen by advection and diffusion

$$\phi \frac{\partial [\mathrm{H_2}]}{\partial t} = \vec{\nabla}.\left(D\vec{\nabla}[\mathrm{H_2}]\text{-}\vec{u}[\mathrm{H_2}]\right) + S_{\mathrm{H_2}}, \qquad (7)$$

where D is the diffusion coefficient, and ϕ the porosity. We adopted the values $D=10^{-8}$ m^2 s^{-1} and $\phi=0.1$ (Jupp & Schultz 2004, Perez et al. 2013). We did not take into account the dispersion effects in this single-pass type model where transport is mainly convective in the high-permeability canal and diffusive in the surrounding low-permeability zone. Cast3M is not a reactive code. We have been able to overcome this restriction by including the serpentinization reactions via the modeling of a production term S_{H2} in the hydrogen transport equation (7). This production term is a function of the temperature T and the w/r ratio as described in the thermodynamic model. In our modeling, we take into account only the serpentinization reaction: we assume that the reaction zone at Rainbow is entirely peridotite and that the produced hydrogen does not react during the transport. Furthermore, as the thermo-hydraulic and transport modelings are not coupled but only solved sequentially, the water consumption and heat production of the serpentinization reactions are neglected. Perez (2012) has shown the validity of these assumptions. The hydrogen transport equation (7) is numerically solved in the same way as the mass and energy balance equations (see Eq. (7) in Perez et al. 2013 for more details).

RESULTS AND DISCUSSION

In a first step, equilibrium calculations were performed to calculate H_2 production during seawater-peridotite alteration for temperatures from 25°C to 400°C, and water/rock (*w/r*) mass ratios in the range 0.2-75. As the thermodynamic properties of the polymorphs involved in the serpentinization reactions are relatively insensitive to pressure, all calculations were performed for a pressure of 35 MPa. Figures 2A,B display the evolution of the H_2 production as a function of the temperature and the *w/r* ratio. Figure 2 shows that the calculated hydrogen concentration at equilibrium, denoted by $[H_2]$, varies strongly with temperature. For all values of the *w/r* ratio, $[H_2]$ first increases with temperature, then reaches a peak at $T \sim 320$°C, and finally decreases sharply at higher temperatures. The increase of $[H_2]$ over the temperature interval from $T = 25$°C to $T \sim 320$°C is due to the increase of the formation of magnetite. At temperatures above ~325°C, olivine is in thermodynamic equilibrium with the fluid and with secondary alteration minerals, such that the amount of Fe that is converted to magnetite then drops. At all temperatures, the amount of H_2 produced per kilogram of harzburgite increases with increasing *w/r* ratio (Fig. 2A). In contrast, the resulting hydrogen concentration (expressed in mol per kg of post-reaction residual water) decreases with increasing *w/r* ratio (Fig. 2B), as the amount of fluid is larger at higher *w/r* ratios. The evolution of $[H_2]$ versus T at *w/r* = 1, and versus *w/r* at T = 100, 300, and 350 °C has already been modeled by McCollom & Bach (2009). Our results are in agreement with these previous results, but extend the results for the H_2 production rates to a wider range of temperatures and *w/r* ratios.

In a second step, we performed the thermo-hydraulic simulation of the Rainbow hydrothermal site in the framework of the single-pass model, as previously described. Figures 3A,B display the temperature and scalar velocity fields when the hydrothermal circulation is established, at t=50 years. We see that fresh fluid first enters the domain through the recharge zone, then heats up while it is flowing above the magmatic heat source, and finally exits at high temperature through the central high-permeability discharge zone. The maximum temperature reached by the exiting fluid is 369°C. The scalar velocities are in the range $(0.2\text{-}5)\times10^{-6}$ m s^{-1} and $(1\text{-}5)\times10^{-5}$ m s^{-1}, in the horizontal heating zone and in the vertical canal, respectively. At the top of the discharge zone, the mass flux of the hydrothermal flow reaches values of 300 kg s^{-1}. All these values are in good agreement with those for the temperatures and mass fluxes that have been measured *in situ* at the Rainbow vent site (T_u ~ 360°C and Q_u ~ 490±220 kg s^{-1}), and with the theoretical values deduced from the single-pass model (Darcy velocities in the horizontal heating zone, u_0, and in the discharge zone, u_u, equal to 5×10^{-7} and 3.5×10^{-5} m s^{-1}, respectively, cf. Table 3 and Eqs. (2)-(3) in Jupp & Schultz 2004).

In a third step, we used the thermo-hydraulic results (temperature and velocity fields) to perform the simulation of the production and transport of hydrogen across the Rainbow site. Figures 4A,B display the hydrogen production and concentration fields after 50 years of continuous heat and hydrogen outputs of the hydrothermal site. For this simulation, the parameter A in the temperature-dependent formulation of the serpentinization rate coefficient (cf. Eq. (2)) is chosen equal to 10^{-11} s^{-1}. Comparing Figs 3A and 4A clearly shows that hydrogen is essentially produced in the zone where the temperature is in the range that is relevant for serpentinization reactions, namely, from 250°C to 350°C.The location of this zone has not been imposed *ab initio* but is a result of the simulation. In marked contrast with these results, we observe that the temperature of the fluid moving through the vertical discharge zone is higher than 350°C and clearly out of the temperature range where serpentinization reactions can occur. As a consequence, no hydrogen is produced in the discharge zone. Furthermore, as shown in Fig. 4B, the hydrogen is less concentrated in the high-permeability canal where it is quickly evacuated by the high-velocity flow than in the surrounding low-permeability zone where it has diffused.

Two similar simulations of the production and transport of hydrogen have been performed with two other values of the parameter A: 10^{-10} s^{-1} and 10^{-12} s^{-1}. Figure 5 displays the time-evolution of the maximum H_2 concentration that exits from the hydrothermal system. Each curve corresponds to a particular value of the parameter A. Figure 5 illustrates the high sensitivity of $[H_2]$ to the kinetics of the reaction of serpentinization. Figure 5 shows that $[H_2]$ ~ 16 mmol kg^{-1} during the whole lifetime of the hydrothermal site (several decades or a few hundreds of years) if $A = 10^{-11}$ s^{-1}. This value of $[H_2]$ is in good agreement with the value measured *in situ* (Charlou et al. 2002, 2010, Seyfried et al. 2011). If A is lower than 10^{-11} s^{-1}, the reaction of serpentinization is too slow with respect to the velocity of the flow (cf. $A = 10^{-12}$ s^{-1} in Fig. 5). Only a small quantity of hydrogen travels in the high-permeability canal and the H_2 concentration in the venting fluid is low ($[H_2] < 2$ mmol kg^{-1}). On the contrary, if A is larger than 10^{-11} s^{-1}, the fast reaction of serpentinization produces a high concentration of hydrogen ([H_2] > 70 mmol kg^{-1}) but also consumes quickly a large quantity of harzburgite (cf. $A = 10^{-10}$ s^{-1} in Fig. 5). The resulting decrease with time of the volume of harzburgite available for the reaction induces the decrease of the H_2 concentration. However, even after several decades of serpentinization, the value for [H_2] in the venting fluid still remains higher than its *in situ* measured value.

Experiments performed at 500 bars, and temperatures between 250 and 350°C, whereby the initial grain size (IGS) of natural olivine was in the range 1-150 μm, showed that the serpentinization kinetics for IGS>5μm is inversely proportional to the square of the IGS (Malvoisin et al. 2012). Using the formulation by Rudge et al. 2010, $A=K_0\times(a_0/a)^2$ with $K_0=10^{-6}$ s^{-1} and $a_0=70$ μm (see equation 3 above), the best value estimated from our simulations, $A=10^{-11}$ s^{-1}, thus corresponds to an effective "grain size" a~2 centimeters. This may be seen as the characteristic length scale of *in situ* serpentinization processes.

Our A value ($A=10^{-11}$ s^{-1}) is lower than the value of A used by Emmanuel & Berkowitz (2006) in their model approach ($A=10^{-10}$ s^{-1}). But both of these values are considerably lower than those obtained from laboratory experiments on powders ($A\sim(0.1\text{-}1)\times10^{-6}$ s^{-1}, Martin & Fyfe 1970, Marcaillou et al. 2011, Malvoisin et al. 2012) or on aggregates ($A\sim10^{-9}$ s^{-1}, Malvoisin et al. 2014). In natural systems, *in situ* coarse-grained ultramafic rocks certainly have a much lower reactive surface area than powders or aggregates used in experiments. The values for the parameter A calculated from our model are about one or two orders of magnitude higher than values obtained by Skelton et al. (2005) from *in situ* seismic velocity data: $A\sim(0.2\text{-}2)\times10^{-12}$ s^{-1} for orthopyroxene and olivine, and $(0.2\text{-}2)\times10^{-13}$ s^{-1} for clinopyroxene. Thus, all the values of the parameter A determined from the *in situ* data are several orders of magnitude lower than those obtained from small grain-size experiments. This reflects the larger characteristic length scale of *in situ* serpentinization processes as expected.

Model robustness and uncertainties

In this study, we use a single-pass type thermo-hydraulic model to study hydrogen production through serpentinization at the Rainbow hydrothermal field by coupling thermodynamic and dynamic modeling. Our numerical simulations show that the serpentinization of peridotites is able to sustain high hydrogen production throughout the lifetime of the venting site. The zone where serpentinization occurs is large enough and contains enough harzburgite to produce hydrogen on the whole continuous lifetime of the Rainbow site. Therefore, this thermo-hydraulic model not only successfully reproduces the observed high temperatures and mass flow rate, but also allows to explain the high hydrogen production rates that are necessary to account for the elevated H_2 concentrations measured in the exiting fluids. Nevertheless, the complexity of the system and the lack of data on the subsurface plumbing and hydrologic flow paths require the introduction of simplifying assumptions, just like for any underconstrained natural system which is investigated by means of a modeling approach. These assumptions translate into a set of imposed parameters, whose values are more-or-less uncertain. Therefore, this raises the question of the impacts of these fixed parameters on results and conclusions. In the single-pass configuration however, these various parameters obey simple scaling laws imposed by the mass and energy conservation equations constrained by the discharge yield of the exiting fluids and the temperature data (Jupp and Schultz, 2004). This fact reduces the number of free parameters drastically.

Permeability field

Permeability is a key parameter for determining hydrologic flow paths in subsurface hydrothermal systems. Unfortunately, it is also one of the most ill-determined parameters in natural geologic settings. Our parametric study of the permeability field (Perez et al., 2013) led to the conclusion that a homogeneous permeability field does not exist that would be able to reproduce simultaneously the high exiting temperatures and the high mass flux which characterize the Rainbow site. Instead, we showed that a single-pass model, that is based on the assumption that the hydrothermal circulation preferentially takes place through a deep high-permeability zone, can account for both the high discharge rate and the high temperatures that are observed *in situ* at the vent site. This conclusion is supported by previous studies, which show that localized venting with a high-heat output requires zones with a high permeability to the focus discharge. It might be more easy to explain this by a single-pass model than by high-Rayleigh-number convection in a homogeneous porous medium (Lowell 1991, Lowell et al. 1995).

The permeabilities k_d of the central discharge zone and k_r of the horizontal high-permeability canal can be deduced in a simple way from the geometric parameters of the system using the mass conservation equations:

- k_d is imposed by the mass flow and temperature of the fluids exiting through the central discharge zone of radius R_d: $k_d = \mu_u W_u/\rho_u g(\rho_o-\rho_u)\pi R^2_d$ (see eq. 3 in Jupp & Schultz 2004). Notation is indicated in Table 3.
- k_r is linked to k_d by the mass conservation equation, such that $k_r = k_d R^2_d/2L^2_r$ (eq. 23 in Jupp & Schultz 2004), where L_r is the thickness of the horizontal high-permeability zone at the base of the system.

Therefore, once the various size parameters of the computational domain are defined (see below), the only value that still can be arbitrarily chosen is that of the permeability outside the high-permeability pathways. Sensitivity tests (Perez, 2012) showed that the results of the model are insensitive to this parameter provided that its value is small enough (in practise, two orders of magnitude lower than that of the high-permeability canal). Making the permeability small enough will ensure that the thermo-hydraulic model is in the single-pass mode. It is therefore capable of reproducing the observed high temperature and high discharge yield.

Size of the computational domain and thermal boundary conditions

In a typical situation, a magmatic heat source is located at a depth L_z of 1000 to 2000 m below the seafloor, coinciding with the base of the sheeted dikes and the upper level of the gabbros (Richardson et al. 1987, Nehlig 1994) and has a width R_r of ~ 1000 m (Detrick et al. 1987, Jupp and Schultz 2004). For the Rainbow site, the venting surface area is ~ 20,000 m^2 (which corresponds to R_d=80m), with a distance R between the central discharge zone and the outer recharge area of a few kms. The temperature imposed at the base of the domain facing the heating zone (Fig. 1), typically 500-700°C, corresponds to the transition between brittle (permeable) and ductile (impermeable) rocks (Lister 1974, 1983, Lowell & Burnell 1991). This is in agreement with evidence from metamorphic assemblages and fluid inclusions obtained from both mid-ocean ridges and ophiolites (see Wilcock, 1998 and references therein).

Sensitivity tests (Perez 2012) indicate that the kinetic parameters of the system are quite insensitive to the value of L_z and R, which is in conformity with the expectations for a single-pass configuration. They also show that the radius of the heating zone, R_r, is imposed by the heat output of the hydrothermal system.

Consequently, the only “loose” parameter is the thickness L_r of the horizontal high-permeability pathway at the base of the system, which may vary around a typical value of L_r ~

100 m (Jupp & Schultz 2004). Therefore, the model has been run with three different values of L_r (60 m, 80 m and 240 m) in addition to the chosen value L_r = 160 m, with the aim of evaluating the sensitivity of the model results to this size parameter. Over the range 60 m-160 m, the dynamical behavior of the model changes rather little, and the calculated A parameter varies from A= 4×10^{-11} to A =10^{-11} s^{-1}. For L_r = 240 m, which corresponds to a Rayleigh number in the horizontal high-permeability pathway that is too small, the flow is dominated by isolated rising and falling plumes whose sizes are smaller than the channel thickness L_r. The model is no longer in the single-pass configuration, and is no longer able to reproduce the mass fluxes observed.

Hydrogen production model

Our calculations were performed for rocks with a harzburgitic composition (80 wt% olivine, 15 wt% orthopyroxene, and 5 wt% clinopyroxene). This is the most representative composition for ultramafic rocks exposed to fluid circulation beneath the seafloor (McCollom & Bach 2009). However, serpentinization reactions and hydrogen production vary with the composition of ultramafic rocks. Klein et al. (2013) explored the composition controls on hydrogen production during serpentinization for a large range of initial olivine/pyroxene ratios. Thermodynamic predictions suggest that serpentinization of olivine-rich lithologies produces more hydrogen (up to a factor of 2 to 3). Therefore, one must keep in mind that the results of the present study depends, in a quantitative way, on the assumption regarding the initial composition of the ultramafic rocks undergoing serpentinization at the Rainbow site. The impact of the uncertainty on the initial rock composition on our estimated A parameter, probably less than a factor of 2, remains modest however, considering the fact that the kinetics of serpentinization reactions may vary by orders of magnitude depending on the *in situ* conditions (see Introduction above). It is also worth noting that we neglected hydrogen generation through ferric-serpentine production whereas it is known to lead to significant hydrogen concentrations at low temperature (Klein et al. 2009). An additional simulation using the results of Klein et al. (2009) indicates that the calibration of A with the value of [H_2] measured *in situ* changes from $A= 10^{-11}$ to $A=1.5\times10^{-11}$.

In conclusion, based on the sensitivity tests performed to evaluate the impact of the various uncertainties on the model results, we estimate that the appropriate value of the parameter A, to describe the *in situ* kinetics of serpentinization at the Rainbow hydrothermal site, lies in the range (1-5)×10^{-11} s^{-1}.

CONCLUSION

Most of the modeling studies concerned with mid-ocean ridge hydrothermal systems are "process-oriented" rather than site-specific, illustrating the inadequacy of the available data as a basis for constructing realistic models. However, in addition to its excellent temperature and fluid geochemistry data, which have remained remarkably stable over more than a decade (including unusually high hydrogen concentrations), the Rainbow site has the specificity of benefiting from an accurate flow rate estimate. This important additional constraint has motivated us to tentatively explore the production of hydrogen by serpentinization in this ultramafic-hosted hydrothermal system by coupling thermodynamic and dynamic modeling. This dynamic model builds further on earlier thermo-hydraulic results for this site (Perez et al. 2013), which showed that a homogeneous permeability field does not exist that would be able to reproduce simultaneously the high exiting temperatures and the high mass flux which characterize the Rainbow site, and that a single-pass type model, based on the assumption that the hydrothermal circulation preferentially takes place through a deep high-permeability zone, is required.

The model results show that a first-order kinetic law is a useful representation of the kinetics of serpentinization. Although it certainly does not fully reflect the complexity of surface reactions in nature, it can be used as an effective law at larger scale. The estimated value for the parameter A in the temperature-dependent formulation of the serpentinization rate coefficient lies in the range ~ (1-5)×10^{-11} s^{-1}, which corresponds to an effective "grain size" a~(1-2) cm. This value may be viewed as the characteristic length scale of *in situ* serpentinization processes. The value for A is in agreement with other published modeling studies of natural systems. It lies between the small values determined from *in situ* data for olivine (A ~ (0.2-2)×10^{-12} s^{-1}) and the very high values obtained from small grain-size experiments (A ~ (0.1-1)×10^{-6} s^{-1}).

Finally, our results confirm that the serpentinization of peridotites is able to sustain high hydrogen production rates throughout the lifetime of an ultramafic-hosted system such as the Rainbow site.

Future sophistications could be incorporated into this simplified initial version, in order to carry out process-oriented studies, such as investigating the impact of the feedback of serpentinization reactions on rock mechanical properties (clogging effect, rock expansion, …) and hence on thermics and hydraulics, or the impact of ideal vs non-ideal mixing in the geochemical model.

This highlights the necessity of including the simplified modeling approach proposed in the present study into the emerging computational geoscience methodology, such that a better understanding of the serpentinization process associated with hydrogen production could be achieved in the future.

ACKNOWLEDGMENTS

The authors acknowledge Thomas McCollom for his useful help in building the thermodynamic database for calculations of chemical equilibrium of solid solutions with the computer program EQ3/6. The authors are also thankful to R. Lowell, M. Appold, and two other anonymous reviewers for their suggestions and constructive comments.

REFERENCES

Agrinier P & Cannat M (1997) Oxygen-isotope constraints on serpentinization processes in ultramafic rocks from the Mid-Atlantic Ridge (23°N), 596 pp., Ocean Drilling Program, College Station, TX, United States.

Andreani M, Baronnet A, Boullier A-M, Gratier J-P (2004) A microstructural study of a « crack-seal » type serpentine vein using SEM and TEM techniques. *European Journal of Mineralogy*, **16**, 585-595.

Allen DE & Seyfried Jr. WE (2003) Compositional controls on vent fluids from ultramafic-hosted hydrothermal systems at mid-ocean ridges: An experimental study at 400°C, 500 bars. *Geochimica et Cosmochimica Acta*, **67**(8), 1531-1542.

Allen D & Seyfried Jr. WE (2004) Serpentinization and heat generation: constraints from Lost City and Rainbow hydrothermal systems. *Geochimica et Cosmochimica Acta*, **68**(6), 1347-1354.

Baker ET (2007) Hydrothermal cooling of midocean ridge axes: Do measured and modeled heat fluxes agree? *Earth and Planetary Science Letters*, **263**, 140-150.

Cave RR, German CR, Thomson J, Nesbitt RW (2002) Fluxes to sediments underlying the Rainbow hydrothermal plume at 30°14’N on the Mid-Atlantic Ridge. *Geochimica et Cosmochemica Acta*, **66**(11), 1905-1923.

Charlou JL, Fouquet Y, Bougault H, Donval JP, Etoubleau J, Jean-Baptiste P, Dapoigny A, Appriou P, Rona PA (1998) Intense CH_4 plumes generated by serpentinization of ultramafic rocks at the intersection of the 15°20’ fracture zone and the Mid-Atlantic Ridge. *Geochemica et Cosmochemica Acta*, **62**(13), 2323-2333.

Charlou JL, Donval JP, Fouquet Y, Jean-Baptiste P, Holm N (2002) Geochemistry of high H_2 and CH_4 vent fluids issuing from ultramafic rocks at the Rainbow hydrothermal field (36°14’N, MAR). *Chemical Geology,* **191**, 345-359.

Charlou JL, Donval JP, Konn C, Ondreas H, Fouquet Y (2010) High production and fluxes of H_2 and CH_4 and evidence of abiotic hydrocarbon synthesis by serpentinization in ultramafic-hosted hydrothermal systems on the Mid-Atlantic Ridge. *AGU Geophysical Monograph Series*, **188**, 265-296.

Delescluse M & Chamot-Rooke N (2008) Serpentinization pulse in the actively deforming

Central Indian Basin. *Earth and Planetary Science Letters*, **276**, 140-151.

Detrick RS, Buhl P, Vera E, Mutter J, Orcutt J, Madsen J, Brocher T (1987) Multi-channel seismic imaging of a crustal magma chamber along the East Pacific Rise. *Nature*, **326**, 35-41.

Douville E, Charlou JL, Oelkers EH, Bienvenu P, Jove Colon CF, Donval JP, Fouquet Y, Prieur D, Appriou P (2002) The Rainbow vent fluids (36°14'N, MAR): the influence of ultramafic rocks and phase separation on trace metal content in Mid-Atlantic Ridge hydrothermal fluids. *Chemical Geology*, **184**(1-2), 37-48.

Emmanuel S & Berkowitz B (2006) Suppression and stimulation of seafloor hydrothermal convection by exothermic mineral hydration. *Earth and Planetary Science Letters*, **243**(3-4), 657-668.

Frost BR (1985) On the Stability of Sulfides, Oxides, and Native Metals in Serpentinite. *Journal of Petrology*, **26**(1), 31-63.

German CR, Klinkhammer GP, Rudnicki MD (1996) The Rainbow Hydrothermal Plume, 36°15'N, MAR. *Geophysical Research Letters*, **23**(21), 2979-2982.

German CR, Thurnherr AM, Knoery J, Charlou JL, Jean-Baptiste P, Edmonds HN (2010) Heat, volume and chemical fluxes from submarine venting: A synthesis of results from the Rainbow hydrothermal field, 36°N MAR. Deep Sea Research Part I: Oceanographic Research Papers **57**(4), 518-527.

Helgeson HC, Kirkham DH, Flowers GC (1981) Theoretical prediction of the thermodynamic behavior of aqueous electrolytes at high pressures and temperatures: IV. Calculation of activity coefficients, osmotic coefficients, and apparent molal and standard and relative partial molal properties to 600°C and 5Kb. *American Journal of Science* **281**, 1249-1516.

Iyer K, Austrheim H, John T, Jamtveit B (2008a) Serpentinization of the oceanic lithosphere and some geochemical consequences: Constraints from the Leka Ophiolite Complex, Norway. *Chemical Geology*, **249**, Issues 1-2, 66-90.

Iyer K, Jamtvei, B, Mathiesen J, Malthe-Sørenssen A, Feder J (2008b) Reaction-assisted hierarchical fracturing during serpentinization. *Earth and Planetary Science Letters*, **267**, Issues 3-4, 503-516.

Iyer K, Rüpke LH, Morgan JP (2010) Feedbacks between mantle hydration and hydrothermal convection at ocean spreading centers. *Earth and Planetary Science Letters*, **296**(1-2), 34-44.

Jamtveit B, Austrheim H, Malthe-Sorenssen A (2000) Accelerated hydration of the Earth's deep crust induced by stress perturbations. *Nature*, **408**, 75-79.

Janecky DR & Seyfried Jr. WE (1986) Hydrothermal serpentinization of peridotite within the oceanic crust: Experimental investigations of mineralogy and major element chemistry. *Geochimica et Cosmochimica Acta*, **50**(7), 1357-1378.

Jean-Baptiste P, Bougaul, H, Vangriesheim A, Charlou JL, Radford-Knoery J, Fouquet Y, Needham D, German CR (1998) Mantle ^{3}He in hydrothermal vents and plume of the Lucky Strike site (MAR 37°17'N) and associated geothermal heat flux. *Earth and Planetary Science Letters*, **157**, 69-77.

Jean-Baptiste P, Fourré E, Charlou JL, German CR, Radford-Knoery J (2004) Helium isotopes at the Rainbow hydrothermal site (Mid-Atlantic Ridge, 36°14'N). *Earth and Planetary Science Letters*, **221**(1-4), 325-335.

Johnson JW, Oelkers EH, Helgeson HC (1992) SUPCRT92: A software package for calculating the standard molal thermodynamic properties of minerals, gases, aqueous species, and reactions from 1 to 5000 bar and 0 to 1000°C. *Computers & Geosciences*, **18**(7), 899-947.

Jupp TE & Schultz A (2004) Physical balances in subseafloor hydrothermal convection cells. Journal of Geophysical Research **109**, B05101, doi:10.1029/2003JB002697.

Kelemen PB & Matter J (2008) In situ carbonation of peridotite for CO_2 storage. Proceedings of the National Academy of Sciences of the United States of America, **105**(45), 17295-17300.

Kelemen PB & Hirth G (2012) Reaction-driven cracking during retrograde metamorphism: olivine hydration and carbonation. *Earth and Planetary Science*, **345-348**, 81-89.

Klein F, Bach W, Joens N, McCollom T, Moskowitz B, Berquo T (2009) Iron partitioning and hydrogen generation during serpentinization of abyssal peridotites from 15 degrees_N on the Mid-Atlantic Ridge. *Geochim. Cosmochim. Acta* **73**, 6868-6893.

Klein F, Bach W, McCollom TM (2013) Compositional controls on hydrogen generation during serpentinization of ultramafic rocks. *Lithos*, **178**, 55-69.

Klein F, Grozeva NG, Seewald JS, McCollom TM, Humphris SE, Moskowitz B, Berquo TS, Kahl WA (2015). Experimental constraints on fluid-rock reactions during incipient serpentinization of harzburgite. *American Mineralogist*, **100**, 991-1002.

Kuznetsov V, Cherkashev G, Lein A, Shilov V, Maksimov F, Arslanov Kh, Stepanova T, Baranova N, Chernov S, Tarasenko D (2006) ^{230}Th/U dating of massive sulfides from the Logatchev and Rainbow hydrothermal fields (Mid-Atlantic Ridge). *Geochronometria,* **25**, 51-55.

Lalou C, Reyss JL, Brichet E (1998) Age of sub-bottom sulfide samples at the TAG active mound. In: *Proceedings of the Ocean Drilling Program, Scientific Results*, **158**, edited by Herzig PM, Humphris SE, Miller DJ, and Zierenberg RA, 111-117.

Lartaud F, de Rafelis M, Oliver G, Krylova E, Dyment J, Ildefonse B, Thibaud R, Gente P, Hoisé E (2010) Fossil clams from a serpentinite-hosted sedimented vent field near the active smoker complex Rainbow, MAR, 36°13’N : Insight into the biogeography of vent fauna. *Geochemistry, Geophysics, Geosystems*, **11**, doi:10.1029/2010GC003079.

Lister CRB (1974) On the penetration of water into hot rocks. .*Geophys. J. R. Astron. Soc.*, **39**, 465-509.

Lister,C . R. B., The basic physics of water penetration into hot rocks,in : Hydrothermal Processes at Seafloor SpreadingCenters,edited by P.A. Rona et al., pp. 141-168, Plenum, New York, 1983.

Liu L & Lowell RP (2009) Models of hydrothermal heat output from a convecting, crystallizing, replenished magma chamber beneath an oceanic spreading center. *Journal of Geophysical Research*, **114**, BO2102, doi:10.1029/2008JB005846.

Lowell RP (1991) Modeling continental and submarine hydrothermal systems. *Reviews of Geophysics*, **29**, 457-476.

Lowell RP and Burnell DK (1991) Mathematical modeling of conductive feat transfer from a freezing, convecting magma chamber to a single-pass hydrothermal system: implications for seafloor black smokers. Earth Planet. Sci. Lett., **104**, 59-69.

Lowell RP, Rona, PA, Von Herzen RP (1995) Seafloor hydrothermal systems. *J. Geophys. Res.*, **100**, 327-352.

Lowell RP & Germanovitch LN (2004) Seafloor hydrothermal processes: Results from scale analysis and single-pass models. In: Mid-Ocean Ridges: hydrothermal interactions between the lithosphere and oceans. *Geophys. Monogr. Ser.*, **148**, edited by German

CR, Lin J, Parson LM, 219-244, AGU, Washington, D.C.

Lowell RP, Farough A, Hoover J, Cummings K (2013) Characteristics of magma-driven hydrothermal systems at oceanic spreading centers. *Geochemistry, Geophysics, Geosystems*, **14**(6), 1756-1770.

MacDonald AH & Fyfe WS (1985) Rate of serpentinization in seafloor environments. *Tectonophysics*, **116**(1-2), 123-135.

Malvoisin B, Brunet F, Carlut J, Rouméjon S, Cannat M (2012) Serpentinization of oceanic peridotites: 2. Kinetics and processes of San Carlos olivine hydrothermal alteration. *Journal of Geophysical Research*, **117**(B4), B04102.

Malvoisin B & Brunet F (2014) Water diffusion-transport in a synthetic dunite: Consequences for oceanic peridotite serpentinization. *Earth and Planetary Science Letters*, **403**, 263-272.

Marcaillou C, Munoz M, Vidal O, Parra T, Harfouche M (2011) Mineralogical evidence for H_2 degassing during serpentinization at 300 °C/300 bar. *Earth and Planetary Science Letters*, **303**(3-4), 281-290.

Marques AF, Barriga F, Chavagnac V, Fouquet Y (2006) Mineralogy, geochemistry, and Nd isotope composition of the Rainbow hydrothermal field, Mid-Atlantic Ridge. *Mineralium Deposita*, **41**(1), 52-67.

Martin B & Fyfe WS (1970) Some experimental and theoretical observations on the kinetics of hydration reactions with particular reference to serpentinization. *Chemical Geology*, **6**, 185-202.

McCaig AM, Cliff RA, Escartin J, Fallick AE, MacLeod CJ (2007) Oceanic detachment faults focus very large volumes of black smoker fluids. *Geology*, **35**(10), 935-938.

McCollom TM & Bach W (2009) Thermodynamic constraints on hydrogen generation during serpentinization of ultramafic rocks. *Geochimica et Cosmochimica Acta*, **73**(3), 856-875.

Moody JB (1976) Serpentinization: A review. *Lithos*, **9**(2), 125-138.

Nehlig P (1994) Fracture and permeability analysis in magma-hydrothermal transition zones in the Samail ophiolite (Oman).). *J. Geophys. Res.*, **99**, 589-601.

Okamoto A, Ogasawara Y, Ogawa Y, Tduchiya N (2011) Progress of hydration reactions in olivine-H_2O and orthopyroxene-H_2O systems at 250°C and vapor-saturated pressure. *Chemical Geology*, **289**, 245-255.

Ogasawara Y, Okamoto A, Hirano N, Tsuchiya N (2013) Coupled reactions and silica diffusion during serpentinization. *Geochimica et Cosmochimica Acta*, **119**, 212-230.

Perez F (2012) Production d'hydrogène par la serpentinisation des roches mantelliques. Apport de la modélisation à la compréhension des processus physiques et géochimiques. PhD thesis of the University of Bretagne Occidentale, France.

Perez F, Mügler C, Jean-Baptiste P, Charlou JL (2013) Coupled modeling of thermics and hydrogeology with the Cast3M code: application to the Rainbow hydrothermal field (Mid-Atlantic Ridge, 36°14'N). *Computational Geosciences*, **17**, 217-237.

Plümper O, Røyne A, Magrasó A, Jamtveit B (2012) The interface-scale mechanism of reaction-induced fracturing during serpentinization. *Geology* **40**(12), 1103-1106.

Richardson CJ, Cann JR, Richards HG, Cowan JG (1987). Metal-depleted root zones of Troodos ore-forming hydrothermal sustems, Cyprus. *Earth Planet. Sci. Lett.*, **84**, 243-253.

Rudge JF, Kelemen PB, Spiegelman M (2010) A simple model of reaction-induced cracking applied to serpentinization and carbonation of peridotite. *Earth and Planetary Science Letters*, **291**(1-4), 215-227.

Seyfried Jr. WE, Foustoukos DI, Fu Q (2007) Redox evolution and mass transfer during serpentinization: An experimental and theoretical study at 200°C, 500 bar with implications for ultramafic-hosted hydrothermal systems at Mid-Ocean Ridges. *Geochimica et Cosmochimica Acta*, **71**, 3872-3886.

Seyfried Jr. WE, Pester NJ, Ding K, Rough M (2011) Vent fluid chemistry of the Rainbow hydrothermal system (36°N, MAR): Phase equilibria and in situ pH controls on subseafloor alteration processes. *Geochimica et Cosmochimica Acta*, **75**(6), 1574-1593.

Skelton A, Whitmarsh R, Arghe F, Crill P, Koyi H (2005) Constraining the rate and extent of mantle serpentinization from seismic and petrological data: implications for chemosynthesis and tectonic processes. *Geofluids*, **5**, 153-164.

Thurnherr AM & Richards KJ (2001) Hydrography and high-temperature heat flux of the Rainbow hydrothermal site (36°14N, Mid-Atlantic Ridge). *Journal of Geophysical Research*, **106**, 9411-9426.

Wegner WW & Ernst WG (1983) Experimentally determined hydration and dehydration reaction rates in the system MgO-SiO_2-H_2O. *American Journal of Science*, **283**-A, 151-180.

Wichers S, Reves-Sohn R, Terray G (2005) New constraints on the thermal power of the TAG hydrothermal system and the dynamics of the water column plume. Eos Trans. AGU 86 Fall Meet. Suppl. (Abstract OS33A-1466).

Wilcock WSD (1998) Cellular convection models of mid-ocean ridge hydrothermal circulation and the temperatures of black smoker fluids. *J. Geophys. Res.*, **103**, 2585-2596.

Wolery TJ (1992) EQ3/6, A Software Package for Geochemical Modeling of Aqueous Systems: Package Overview and Installation Guide (Version 7.0), Lawrence Livermore National Laboratory, Livermore, CA.

Component	Cl^-	Na^+	Mg^{2+}	K^+	HCO_3^-	$SiO_{2(aq)}$	Al^{3+}	Ca^{2+}	Fe^{2+}	SO_4^{2-}	$O_{2(aq)}$	H_2	pH	Eh (V)
Concentration (mmolal)	545.4	464.0	37.0	9.8	2.3	0.16	2×10^{-5}	10^{-5}	1.5×10^{-6}	0	0	0	7.7	0.275

Table 1: Initial fluid composition used in the model.

Solid solution	Components
Olivine $(Fe,Mg)_2SiO_4$	Fayalite and Forsterite
Orthopyroxene $(Fe,Mg)SiO_3$	Enstatite and Ferrosilite
Clinopyroxene $Ca(Fe,Mg)Si_2O_6$	Diopside and Hedenbergite
Serpentine $(Fe,Mg)_3Si_2O_5(OH)_4$	Chrysotile and Greenalite
Brucite $(Mg,Fe)OH_2$	Brucite and $Fe(OH)_2$
Talc $(Fe,Mg)_3Si_4O_{10}(OH)_2$	Talc and Minnesotaite
Amphibole $Ca_2(Fe,Mg)_5Si_8O_{22}(OH)_2$	Tremolite and Ferrotremolite

Table 2: List of solid solutions included in the thermodynamic database.

Notation	Definition	Values deduced from Rainbow data	Values deduced from the single-pass model
S_d	Surface of the hot-fluid discharge zone	20,000 m^2	
L_z	Domain thickness	1400 m	
W_u	Mass flux of high-temperature vent fluids	490 ± 220 kg s^{-1}	
$Q_u=W_u/S_d$	Mass flux per square meter	2.45×10^{-2} kg s^{-1} m^{-2}	
T_u	Maximum temperature of the vent fluids	360°C	
ρ_u	Density of the upflowing fluid at (P, T) = (390 bars, 360°C)	700 kg m^{-3}	
μ_u	Dynamic viscosity of the upflowing fluid	7×10^{-5} kg m^{-1} s^{-1}	
$c_p(T_u)$	Heat capacity of upflowing fluid at (P, T) = (390 bars, 360°C)	6000 J kg^{-1} K^{-1}	
h_u	Specific enthalpy of upflowing fluid	3.8×10^{6} J kg^{-1}	
ρ_0	Density of the cold fluid at (P, T) = (390 bars, 2°C)	1000 kg m^{-3}	
μ_0	Dynamic viscosity of the cold fluid at (P, T) = (390 bars, 2°C)	1.6×10^{-3} kg m^{-1} s^{-1}	
$c_p(T_0)$	Heat capacity of the cold fluid at (P, T) = (390 bars, 2°C)	4000 J kg^{-1} K^{-1}	
h_0	Specific enthalpy of the cold fluid $h_0 = c_p(T_0) \times T_0$	1.1×10^{6} J kg^{-1}	
T_m	Maximum temperature of the fluid due to the presence of the magma		600°C
λ	Crust's thermal conductivity		2 W m^{-1} K^{-1}
R_d	Radius of the hot-fluid discharge zone		80 m
R_r	Radius of the heating zone above the magmatic body		1320 m
L_r	Thickness of the heating zone		160 m
δ_r	Thickness of the conductive boundary layer in the heating zone		2 m
k_d	Permeability in the discharge zone		8×10^{-13} m^2
k_r	Permeability in the heating zone		10^{-13} m^2

Table 3: Description of the different parameters of the single-pass model and corresponding values obtained from measurements and theoretical formulations for the Rainbow hydrothermal site.

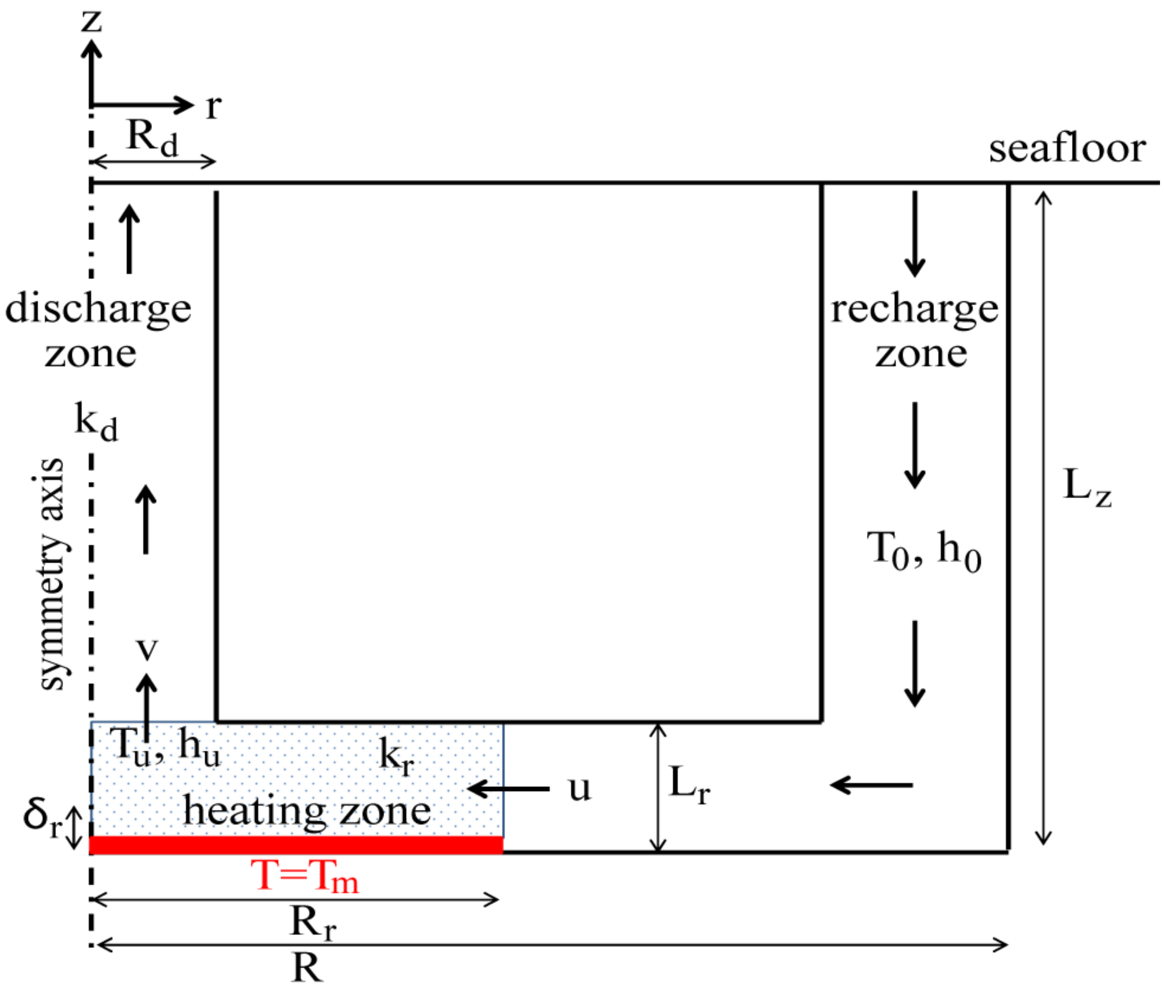

Figure 1: Configuration of the single-pass geometry used to model the Rainbow vent site.

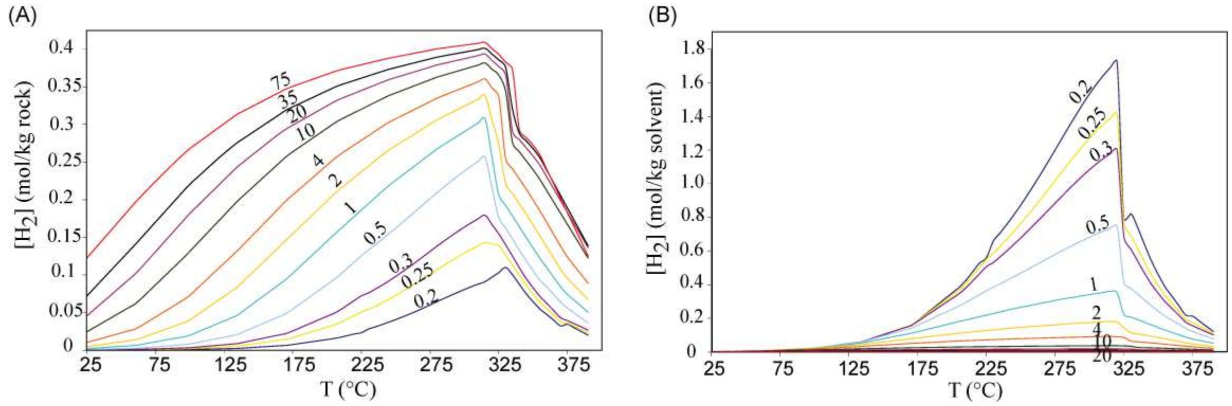

Figure 2: H_2 production as a function of the temperature T (°C), and for various values of the water/rock ratio ($0.2 < w/r < 75$). The concentration [H_2] is expressed in mol per kg of initial harzburgite (A), and mol per kg of water remaining after reaction (B).

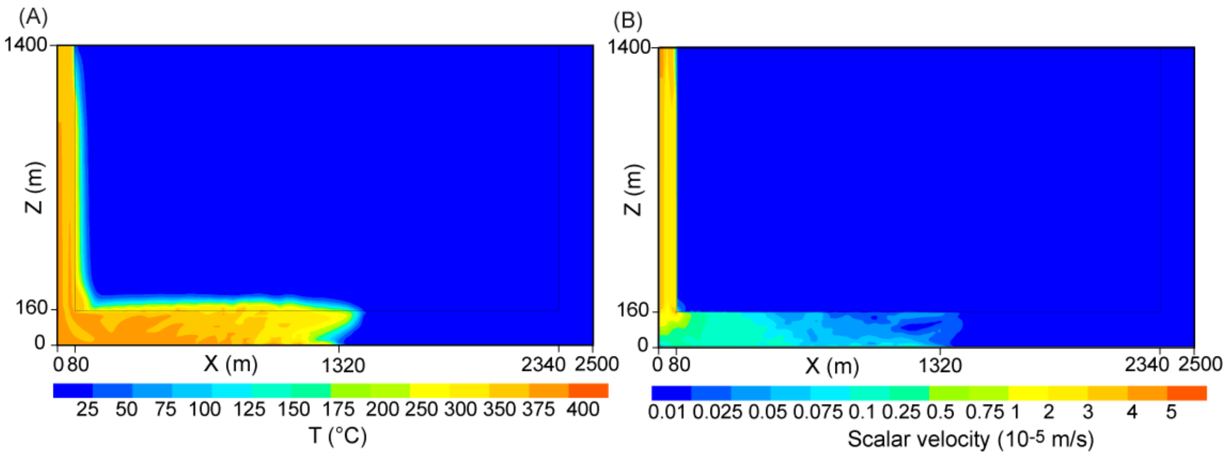

Figure 3: Modeling of the Rainbow vent site with an axisymmetric single-pass geometry. Snapshots of the vertical fields of the temperature (A), and the scalar velocity (B), when the hydrothermal circulation is established.

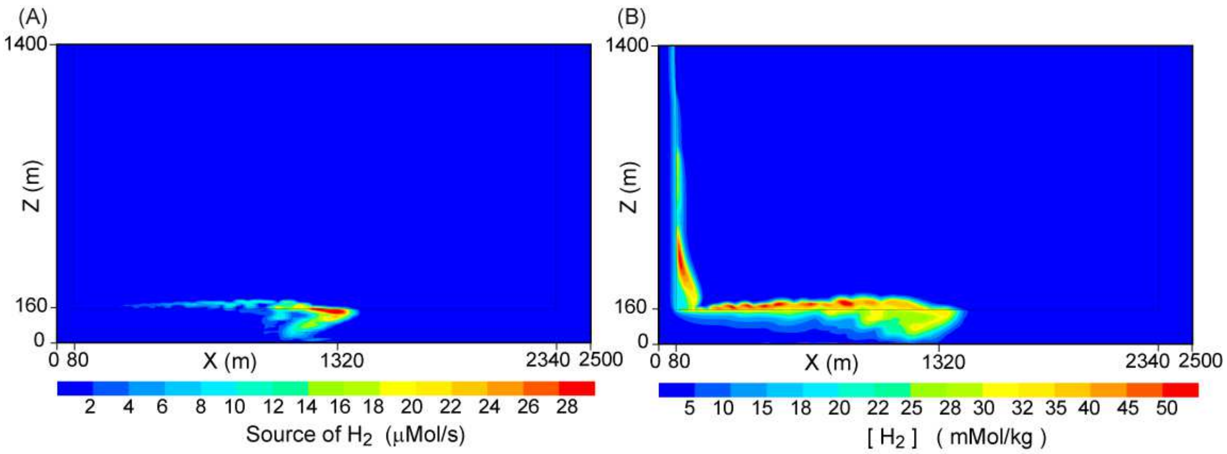

Figure 4: Modeling of production and transport of hydrogen at the Rainbow vent site with an axisymmetric single-pass geometry. Snapshots of the vertical fields of the source (A), and the concentration of hydrogen (B), when the hydrothermal circulation is established.

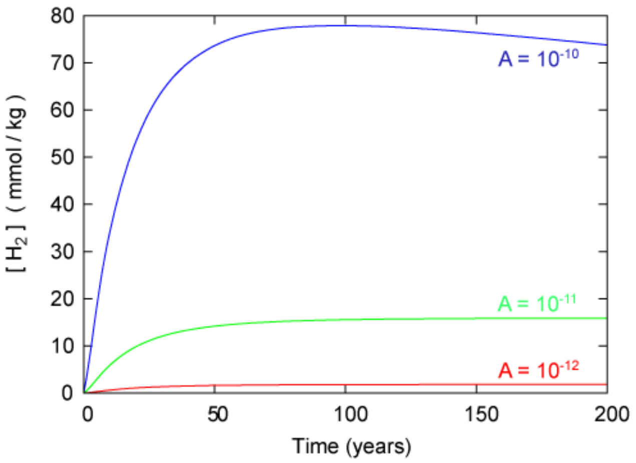

Figure 5: Time evolution of the maximum hydrogen concentration that exits from the hydrothermal system, for three different values of the serpentinization rate coefficient.